PAPER

Check for updates

Tailoring adsorbents for levodopa detection: a DFT study on Pt-encapsulated fullerene systems†

Wendy Maxakato,[a] Miracle N. Ogbogu,[b] Adebayo P. Adeleye, [ID] *[cd]
Ismail O. Amodu, [ID] [e] Innocent Benjamin [ID] *[f] and Henry O. Edet [ID] [g]

Despite its effectiveness in managing the motor symptoms of Parkinson's disease, levodopa therapy is often accompanied by adverse effects that can significantly reduce patients' quality of life. Hence, the need to detect levodopa has escalated among researchers and health experts. Herein, the intricacies of levodopa adsorption were studied using newly tailored fullerene-based adsorbents. All theoretical calculations were performed using the DFT/PBE1PBE/GENECP level of theory. Having modified the surface by Pt-encapsulation followed by functionalization with a functional group ($COOH$, HCO, NH_2, NO_2, and OH), new materials were engineered towards levodopa adsorption. Various theoretical and computational analyses were thoroughly explored to gain insight into the electronic properties, nature of inter- and intra-molecular interactions, strength and phenomenal of adsorption, and the mechanisms of sensing. Adsorption was found to have taken place from the region of the functional groups, where adsorption strength is influenced by the varying electron-withdrawing abilities of the groups. In all cases, the adsorption phenomenon is best described as physisorption. Changes in the dimensions are attributed to the stretching vibration of the bonds on the surface. Also, the small energy gaps within a close range of 0.295 to 0.675 eV exhibited by the materials upon adsorption are an indication of semiconductors. Hence, the functionalized systems hold promise as adsorbents for levodopa molecules, offering valuable insights for future research endeavors.

1   Introduction

One of the most commonly used drugs in the treatment of Parkinson's disease is levodopa.[1] This disease, characterized as a neurodegenerative disorder, is accompanied by several motor disabilities (bradykinesia and dyskinesia) and tremors that continuously cause death of nerve cells and impair speech in affected patients.[2,3] The risks to patients suffering from this disorder can be life threatening, necessitating a critical advancement in pharmacotherapy for the development of various restorative drugs, procedures, and methods for increasing the lifespan of these patients.[4,5] After approval by the FDA in 1975,[6] levodopa has been administered for treating

Parkinson's disease symptoms due to its potential to bypass various barriers from the blood to the brain.[7] A major precursor of levodopa is the release of dopamine after the blood–brain barrier has been crossed. The dopamine produced serves as an active stimulant for dopaminergic receptors.[8,9] Despite its clinical advantages, patients receiving levodopa administration exhibit different side effects, such as hypertensive crises, somnolence, excessive sleepiness, and a reduction in quality of life.[9,10] In a clinical trial of levodopa in pregnant rabbits, the litters were oddly smaller in size and had developed some skeletal deformities; hence, there is a need for more studies on its effect on humans and possible modifications for more effective results.[11,12] Due to this effect, the detection of levodopa in the body has become essential to researchers and scientists.

In recent years, the utilization of carbon-based materials has attracted significant attention in various pharmaceutical, industrial, medical, agricultural, and environmental fields due to their unique properties and diverse applications.[13] Among these materials, C_{60}, also known as buckminsterfullerene, has emerged as a promising candidate for surface modification and functionalization due to its exceptional stability, high surface area, and molecular encapsulation capabilities.[14,15] C_{60} has been utilized in various studies for standard surface modification and functionalization of various substrates to explore its potential as an adsorbent.[16] The choice of C_{60} as the standard surface in this

[a]Department of Chemical Sciences, University of Johannesburg, Johannesburg, South Africa

[b]Department of Genetics and Biotechnology, University of Calabar, Calabar, Nigeria

[c]Department of Chemistry, Federal University of Technology, Akure Ondo, Nigeria. E-mail: adeleyepauladebayo36@gmail.com

[d]Department of Chemistry, Marquette University, Milwaukee, WI, USA

[e]Department of Mathematics, University of Calabar, Calabar, Nigeria

[f]Department of Microbiology, University of Calabar, Calabar, Nigeria. E-mail: benjamininnocent53@gmail.com

[g]Department of Biochemistry, Cross River University of Technology, Calabar, Nigeria

† Electronic supplementary information (ESI) available. See DOI: https://doi.org/10.1039/d4ra03526g

investigation stems from several advantageous properties such as its excellent chemical stability among many others, which ensures the robustness of the modified surfaces under diverse environmental conditions.[17,18] Additionally, its high surface area provides ample opportunities for the attachment of functional groups and molecules, facilitating tailored surface modifications.[18] Moreover, the unique cage-like structure of C_{60} allows for the encapsulation of guest molecules within its framework, offering additional functionalities and enhancing the adsorption properties of the modified surfaces.[19] Due to this effect, this present work designed new fullerene-based materials by encapsulation and functionalization to form the platinum-encapsulated, X-functionalized fullerene C_{60} adsorbent materials.

According to Martinez, systems that interact strongly with dopamine may be agonistic and may interfere with its delivery at the receptor site because they are good electron donors, such as dopamine.[1] It was observed that systems with boron form stable structures but might serve better as antipsychotics than delivery systems for dopamine. Additionally, Raghu *et al.* reported that BCN (boron carbonitride) serves as a good electrode material in supercapacitors and electrocatalysts for analysing biological samples for the detection of levodopa.[2] Duhan and Obrai observed that the fluorescence intensity of nitrogen sulfur codoped graphene quantum dots (NSGQDs) decreased as the concentration of levodopa increased, and this fluorescence showed greater specificity for L-DOPA.[3] In a study carried out by Alsubaiyel, Amal M., *et al.* on a theoretical investigation of the adsorption and electronic properties of bare and Al-doped C_{60} fullerenes, the adsorption of N_2O molecule was carried out and the result showed that based on the binding energy of the range of 0.2–41.2 kJ mol^{-1} and the large electronic charge transfer between Al@C_{59} fullerene surface and N_2O, the Al@C_{59} is a suitable N_2O gas-sensing material.[20] In furtherance, Hamid Hadi and coworkers investigated the sensing capabilities of pristine and doped C_{60} fullerene towards methamphetamine (MAT) using density functional theory (DFT). Zn-doped C_{60} fullerene showcased the most favourable sensing attributes as a result of its highest reactivity and adsorption energy of −45.02 kcal mol^{-1}. These studies highlighted the potential modified C_{60} fullerene as adsorbents or drug carriers. Hence, they justify the structural modification performed in this present study.[21]

In this comprehensive study, we systematically explored the modification of C_{60} fullerene surfaces through encapsulation and functionalization with various functional groups, including carboxyl (COOH), formyl (HCO), amino (NH_2), nitro (NO_2), and hydroxyl (OH) moieties.[19] The encapsulation carried out involves placing a potential atom inside of the cage-like structure of C_{60} fullerene,[22] while functionalization, unlike decoration involves bonding functional group to the surface without replacing them, but alters the morphology of the parent surface.[23] By employing these methods, we aim to tailor the surface properties of C_{60} and investigate their effects towards the detection of levodopa. The adsorption ability of each modified surface was evaluated, aiming to elucidate the influence of different functional groups on the adsorption efficiency and selectivity of the substrates.[24] Interestingly, a detailed analysis of the adsorption behavior of these functionalized surfaces will provide valuable insights into

their potential as an adsorbent for pharmaceuticals.[25,26] Firstly, analysing the bond lengths and angles provides insights into the structural changes induced by surface modifications, aiding in understanding the underlying mechanisms governing adsorption phenomena.[22] Levodopa (LDP), an absorbate known for its potential therapeutic applications, served as a test material in this study. Levodopa complexes, including LDP-COOH-Pt@C_{60}, LDP-HCO-Pt@C_{60}, LDP-NH$_2$-Pt@C_{60}, LDP-NO$_2$-Pt@C_{60}, and LDP-OH-Pt@C_{60}, were investigated to assess their adsorption ability in adsorption and sensor applications. The novelty of this study lies in its comprehensive investigation of surface modification techniques applied to C_{60} (endohedral encapsulation and functionalization) and their effects on adsorption behaviour. By elucidating the relationship between surface modifications and adsorption properties, this study aims to contribute to the development of advanced materials for various applications, including sensing and catalysis.

2 Computational methodology

In the present study, the modified fullerene surface and its complexes were sketched and optimized using Gaussview 09 and Gaussian 16 software at the DFT/PBE1PBE/GENECP level of theory.[27] It is noteworthy that the optimization achieves the attainment of the potential energy minimum. First, frontier molecular orbital (FMO) analysis was performed, and orbital differences were used to elucidate the conductive and stable properties of the systems.[28] Additionally, natural bond orbital (NBO) analysis carried out using the NBO 7.1 embedded in the Gaussian package was used to evaluate the stabilization of the systems and charge transfer between the adsorbed levodopa molecule and the modified fullerene systems.[29] The adsorption of the levodopa molecule on the system was computed using eqn (1).[30]

$$E_{ads} = E_{LDP/Fullerene} - (E_{LDP} + E_{Fullerene}) \qquad (1)$$

where $E_{LDP/Fullerene}$ is the energy of the complex formed between the levodopa molecule and the modified fullerene surface, E_{LDP} is the energy of the singly optimized levodopa molecule and $E_{Fullerene}$ is the energy of the optimized fullerene surface.[31] Moreover, the sensor properties, *e.g.*, electrical conductivity, charge transfer and work function, fraction of electron transfer (FET), and back donation, were evaluated to gain insight into the sensing capabilities of the systems.[28] The topology analysis, which describes the nature of the interaction between the levodopa molecule and the fullerene systems, was obtained from the quantum theory of atom in molecules (QTAIM) and the noncovalent interaction (NCI) carried out in multiwfn, and the visualization was performed using visual molecular dynamics (VMD).[32,33] Therefore, for constructing an effective adsorbent for levodopa molecules through a theoretical approach, these objectives make it possible to gain insight into the intricacies of adsorption.

3 Results and discussion

3.1 Structural geometry

The fullerene C_{60} surface, which has a spherical structure and 60 carbon atoms organized in hexagonal and pentagonal rings

with high symmetry, was used in this investigation. Afterwards, the C_{60} surface was modified by endohedral encapsulation with a platinum (Pt) atom.[15] The introduction of the Pt atom was followed by functionalization, with selected functional groups (COOH, HCO, NH_2, NO_2, and OH), which induced significant alterations in its geometric properties, particularly concerning bond changes.[19] The bonding environment changes with the Pt, while the functional groups contribute to the redefined molecular architecture of the fullerene by introducing new bond types, each with its own distinct chemical features.[34] For example, carboxylate functionalities are imparted by COOH, formyl moieties are introduced by HCO, amino groups are brought by NH_2, nitro functionalities are added by NO_2, and hydroxyl groups are brought by OH. These functional groups affect the steric and electrical properties of fullerene in addition to varying the chemical makeup of the bonds.[35] The combination of these changes yields a complex three-dimensional configuration that reflects the complex interaction between Pt doping and various functional groups. Moreover, the adsorbate levodopa, a precursor of dopamine, is composed of an amino group, a hydroxy group, and a benzene ring.[10] The levodopa molecule was adsorbed on the functionalized region of the Pt-encapsulated fullerene surface to evaluate the impact of the considered functional groups on the adsorption or sensing of the studied molecule.

In addition, because the adsorption of levodopa on X-Pt@C_{60} (COOH, HCO, NH_2, NO_2, and OH) surfaces may alter the morphology of the surface, the dimensions of the surface may change as a result of functionalization. These changes have been examined to better understand the nature of their vibrations.[18] Dimensions D were examined before and after functionalization, as well as during adsorption. Changes in the dimensions of the complexes were observed after adsorption, and these changes were found to be significant.[22] The difference in diameter may be checked so that a change in the surface morphology may be observed. Fig. 1 shows the dimensions of the modified surfaces before and after functionalization,

whereas Fig. 2 shows the structures of the systems, levodopa molecules, and complexes formed. Upon functionalization, the dimensions increased from 7.02 Å in Pt@C_{60} to 7.35 Å (4.7%), 7.15 Å (1.9%), 7.39 Å (5.3%), 7.31 Å (4.1%), and 7.38 Å (5.1%), corresponding to COOH-Pt@C_{60}, HCO-Pt@C_{60}, NH_2-Pt@C_{60}, NO_2-Pt@C_{60}, and OH-Pt@C_{60}, respectively. Upon adsorption, the dimensions increased to 7.35 Å, 7.31 Å, 7.39 Å, 7.31 Å, and 7.39 Å for LDP-COOH-Pt@C_{60}, LDP-HCO-Pt@C_{60}, LDP-NH_2-Pt@C_{60}, LDP-NO_2-Pt@C_{60}, and LDP-OH-Pt@C_{60}, respectively. These changes in the dimensions are attributed to the stretching vibration of the bonds in which the surfaces are made.

3.2 Electronic properties

3.2.1 Quantum descriptors. With the aim of building an effective adsorbent or sensing material for levodopa, a precursor of dopamine, the energies of the frontier molecular orbital, HOMO, and LUMO provide insights into the stable and conductive properties of the proposed fullerene-based adsorbent, Pt@C_{60}, with its functionalized counterparts. COOH-Pt@C_{60}, HCO-Pt@C_{60}, NH_2-Pt@C_{60}, NO_2-Pt@C_{60} and OH-Pt@C_{60}. In line with previous research, the presence of a high energy gap signifies more stable and less reactive systems, whereas a lower energy gap indicates a less stable and more reactive system. In,[28] frontier molecular orbital analysis was employed to elucidate the properties of their model system for their respective applications.[36,37] Herein, the studied systems optimized at the DFT/PBE1PBE/GENECP level of theory were evaluated, and the obtained results are presented in Table 1. The pristine Pt@C_{60} surface exhibited an E_g of 2.238 eV, which indicates its conductive properties. However, upon functionalization with COOH, HCO, NH_2, NO_2, and OH groups, a reduction in the energy gap is obtained. HCO-Pt@C_{60} has a much lower energy gap of 1.756 eV, while energy gaps of 1.994 eV and 1.999 eV are observed for NO_2-Pt@COOH and OH-Pt@COOH, respectively. For the functionalized systems, HCO-Pt@C_{60} was the most conductive, which could be due to the presence of a formyl group, which plays a crucial role in the structure and
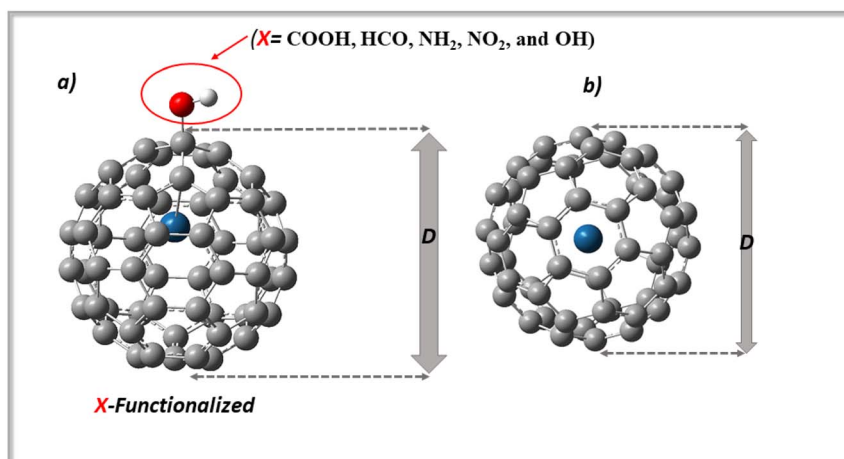

Fig. 1 Optimized structures of (a) the adsorbed Cu-Pt@C_{60} and (b) the bare Cu-Pt@C_{60} surface, showing the diameter (*D*) and adsorption distance (*d*).
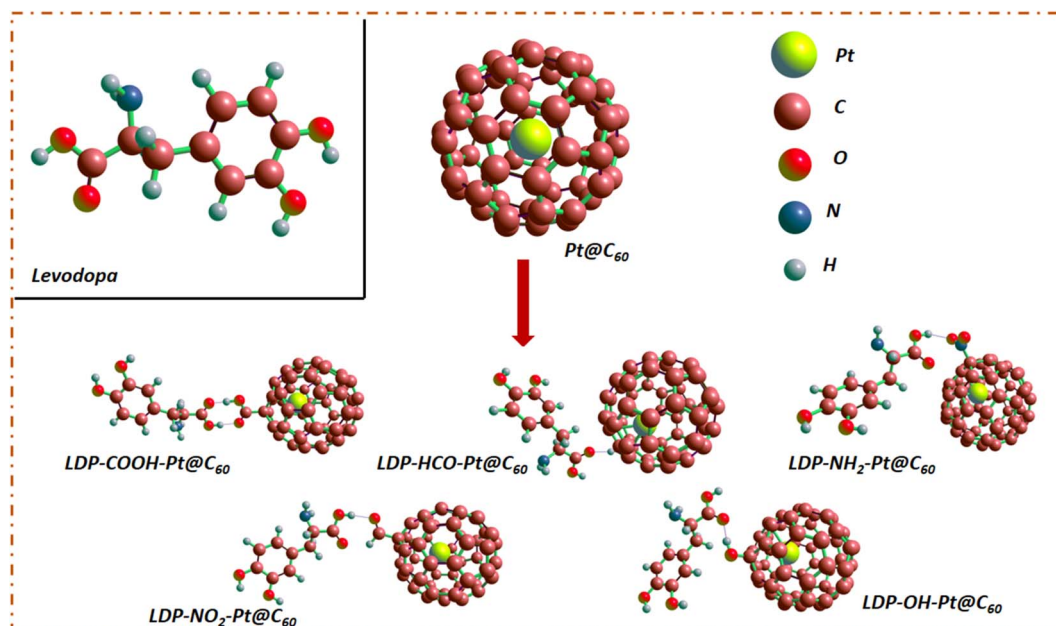
Fig. 2 Structural view of the encapsulated fullerene, functionalized models and complexes, and levodopa molecule.

Table 1 The calculated HOMO and LUMO energies and quantum descriptors for the isolated and adsorbed systems calculated at DFT/PBE1PBE/GENECP level of theory

System	E_{HOMO} eV	E_{LUMO} eV	E_g eV	μ (eV)	η (eV)	S (eV^{-1})	ω (eV)
Pt@C$_{60}$	−5.860	−3.622	2.238	4.745	1.119	0.447	10.041
COOH-Pt@C$_{60}$	−9.536	−7.484	2.052	8.510	1.025	0.487	35.295
HCO-Pt@C$_{60}$	−9.456	−7.700	1.756	8.578	0.878	0.569	41.902
NH$_2$-Pt@C$_{60}$	−9.469	−7.434	2.035	8.451	1.018	0.491	35.095
NO$_2$-Pt@C$_{60}$	−9.753	−7.758	1.994	8.755	0.997	0.501	38.438
OH-Pt@C$_{60}$	−9.544	−7.545	1.999	8.544	0.999	0.500	36.520
LDP-COOH-Pt@C$_{60}$	−7.569	−7.274	0.295	7.421	0.147	3.390	186.705
LDP-HCO-Pt@C$_{60}$	−7.693	−7.387	0.306	7.540	0.153	3.264	185.534
LDP-NH$_2$-Pt@C$_{60}$	−7.760	−7.085	0.675	7.423	0.337	1.482	81.644
LDP-NO$_2$-Pt@C$_{60}$	−7.799	−7.384	0.415	7.591	0.207	2.410	138.871
LDP-OH-Pt@C$_{60}$	−7.676	−7.267	0.409	7.471	0.205	2.443	136.398

reactivity of molecules.[38] Nonetheless, upon the adsorption of levodopa, a more conductive complex is formed, indicating good sensing abilities of the functionalized systems. The LDP-COOH-Pt@C$_{60}$, LDP-HCO-Pt@C$_{60}$, LDP-NH$_2$-Pt@C$_{60}$, LDP-NO$_2$-Pt@C$_{60}$ and LDP-OH-Pt@C$_{60}$ systems agree with E_g values of 0.295 eV, 0.306 eV, 0.675 eV, 0.415 eV, and 0.409 eV, respectively. The energy gap (E_g) determines the electrical conductivity of a system in the sense that as the energy gap decreases, the electrical conductivity of the system increases, whereas an increment in the energy gap, causes the electrical conductivity to decrease.[39] According to the results obtained in tandem with previous literature,[40] the studied systems exhibit the potential to serve as adsorbents or sensor materials for levodopa.[24,36] Furthermore, the calculated chemical hardness and softness descriptors are comparable for the systems and complexes, hence supporting the electronic behavior of the systems in this study.

Fig. 3 shows the isosurfaces of the studied systems; these orbitals are evenly distributed across molecular surfaces and complexes, reflecting a balanced electronic configuration. However, an exception is observed in the HCO-Pt-C$_{60}$ complex, where the HOMO is uniquely situated on the encapsulated Pt atom. This typical distribution suggests a pivotal role for the Pt atom in influencing the complex's electronic structure.[22] Furthermore, when the HCO-Pt-C$_{60}$ surface forms a complex with levodopa, the localization of the HOMO on the Pt atom persists, while the LUMO becomes distributed around the surface. This implies two major things (electron donor and orbital overlap). Pt atom having a localized HOMO acts as an electron donor to levodopa. This creates forces of attraction between the positively charged Pt and functional groups in levodopa that can accept electrons, thereby encouraging adsorption. Also, the spread-out LUMO of the surface result in orbital overlap in levodopa, leading to the formation of new
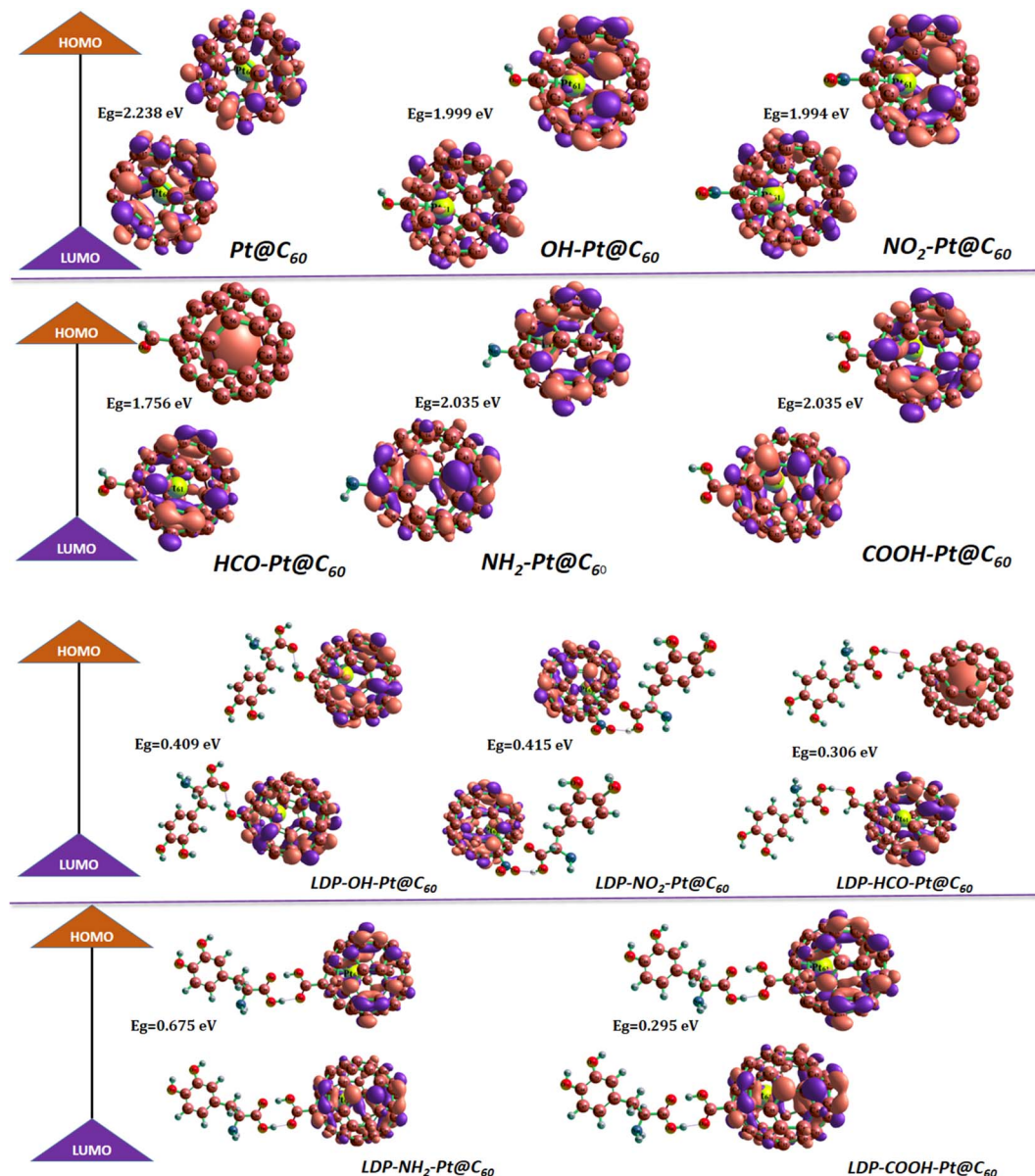
Fig. 3   Molecular orbital surface for systems and complexes.

bonding interactions that hold the levodopa molecule to the surface.

3.2.2   NBO analysis. Conversely, natural bond orbital (NBO) analysis was carried out to confirm the type of donor–acceptor orbital interaction that exists between the adsorbed levodopa molecules on the tailored surfaces.[39] The NBO method is a strategy for simplifying the difficult Schrödinger equation into an understandable chemical bonding idea, and the intermolecular charge transfer and electron delocalization that occur between the adsorbent and adsorbate are also well highlighted by NBO analysis.[41] However, the degree of interaction between the donor and acceptor orbitals is quantified by the stabilization energy E^2. A greater intensity of interaction between these orbitals corresponds to a greater stabilization energy.[36,39] In accordance with prior computational research, the stabilization energy for the most contributing donor–acceptor orbitals in the studied systems, and the results obtained are presented in Table 2. According to the results, the π and LP transitions are dominant in the studied systems. LDP-OH-Pt@C$_{60}$ has a higher E^2 of 2509 kcal mol^{-1} with a transition between LP C1 and LP* C58, which is a charge delocalization resulting from charge transfer from lone pair of carbon atom to anti-bonding character of lone pair of carbon atom, whereas the lowest E^2 of 11.66 kcal mol^{-1} is observed for Pt@C60 between π C59–C60, π* C54 and C55. For the functionalized systems, a comparable stabilization energy is observed, except for COOH-Pt@C$_{60}$, which has the highest E^2 herein, confirming the findings from the FMO analysis. The decreasing order of stabilization energies for the fullerene-based systems and complexes is as follows: LDP-OH-Pt@C$_{60}$ > LDP-COOH-Pt@C$_{60}$ > LDP-NH$_2$-Pt@C$_{60}$ >

Table 2 Most contributing second-order perturbation energies for the studied systems calculated at DFT/PBE1PBE/GENECP level of theory

Systems	Donor (i)	Acceptor (j)	E^2 kcal mol^{-1}	$E(i)$–$E(j)$	$F(i,j)$
Pt@C$_{60}$	π C$_{59}$–C$_{60}$	π^* C$_{54}$–C$_{55}$	11.66	0.32	0.055
COOH-Pt@C$_{60}$	LP O$_{64}$	LP* H$_{65}$	519.43	0.68	0.531
HCO-Pt@C$_{60}$	π C$_4$–C$_9$	π^* C$_{10}$–C$_{11}$	232.10	0.01	0.076
NH$_2$-Pt@C$_{60}$	π^* C$_1$–C$_{58}$	π^* C$_{16}$–C$_{57}$	238.68	0.01	0.077
NO$_2$-Pt@C$_{60}$	π^* C$_{54}$–C$_{55}$	π^* C$_{45}$–C$_{53}$	244.00	0.01	0.076
OH-Pt@C$_{60}$	π^* C$_1$–C$_{58}$	π^* C$_{16}$–C$_{57}$	243.55	0.01	0.077
LDP-COOH-Pt@C$_{60}$	LP C$_1$	LP* C$_{58}$	2013.87	0.02	0.161
LDP-HCO-Pt@C$_{60}$	LP O$_{85}$	LP* H$_{86}$	513.55	0.65	0.519
LDP-NH$_2$-Pt@C$_{60}$	LP C$_4$	LP* C$_9$	2156.44	0.02	0.163
LDP-NO$_2$-Pt@C$_{60}$	LP O$_{85}$	LP* H$_{86}$	515.35	0.65	0.526
LDP-OH-Pt@C$_{60}$	LP C$_1$	LP* C$_{58}$	2509.66	0.01	0.161

COOH-Pt@C$_{60}$ > LDP-NO$_2$-Pt@C$_{60}$ > LDP-HCO-Pt@C$_{60}$ > NO$_2$-Pt@C$_{60}$ > OH-Pt@C$_{60}$ > HCO-Pt@C$_{60}$ > Pt@C$_{60}$. In this context, it is noteworthy that the systems and complexes under consideration exhibit good attributes of a sensing material, wherein the LDP-OH-Pt@C$_{60}$ complex will be easily stabilized during adsorption as compared to its studied counterparts.

3.3 Adsorption studies

The adsorption of levodopa (LDP) on X-functionalized Pt-encapsulated fullerenes (X-Pt@C$_{60}$, where X = COOH, HCO, NH$_2$, NO$_2$, and OH) was investigated in this study. The optimized structures for LDP adsorption on the functionalized surfaces are visualized in Fig. 2, which shows the structural geometry. The calculated adsorption energies show physisorption phenomena of adsorption,[42] which is due to the positive adsorption energy obtained, calculated within a close range of 326.3 to 340.7 kcal mol^{-1}. The results obtained are summarized in Table 3. The presence of weak interactions between the adsorbate and adsorbent was identified from the magnitude of the adsorption energy. The least positive adsorption energy of 326.3 kcal mol^{-1} attributed to LDP-COOH-Pt@C$_{60}$ shows relatively better detection of levodopa than their counterparts. This is because the farther the adsorption energy is from the negative, the weaker it becomes.[31] In the present work, LDP-NH$_2$-Pt@C$_{60}$ showed the largest positive adsorption energy of 340.7 kcal mol^{-1}, suggesting that it had the weakest detection energy for levodopa. Since the energies are relatively close, the detection strength for levodopa follows the pattern LDP-COOH-Pt@C$_{60}$ < LDP-OH-Pt@C$_{60}$ < LDP-NO$_2$-Pt@C$_{60}$ < LDP-NO$_2$-Pt@C$_{60}$ < LDP-NH$_2$-Pt@C$_{60}$, which is a decreasing order of the detection strength (see Table 3). Furthermore, structural modification by functionalization with

the –COOH functional group resulted in better detection, followed by functionalization with the –OH functional group and then functionalization with the –NO$_2$ functional group, as shown in the aforementioned pattern. In general, the presence of close adsorption range of 326.3 to 340.7 kcal mol^{-1} indicates that all tailored materials exhibit a similar pattern of adsorption strength.

3.4 Visual studies

3.4.1 QTAIM. The quantum theory of atoms-in-molecules (QTAIM) proposed by Bader has become an important analysis technique for the study of the intra- and intermolecular interactions occurring in atoms of a compound.[35] This analysis is also regarded as an analysis of weak interactions and consists of different variables that describe the system. Its variables range from the bond critical points (BCPs), which indicate the bonds present, and improve the calculation and prediction of other parameters of the QTAIM. Other topological parameters include the electron density ($H(r)$), Laplacian of electron of electron density $\nabla^2\rho(r)$, Eigenvalues of Hessian, and ellipticity of electro density (e), among others. Table 4 encompasses the parameters of the QTAIM analysis as observed in this study. The highest $\rho(r)$ values observed in the complexes are 0.799 a,u at H$_{73}$–N$_{88}$ for LDP-COOH-Pt@C$_{60}$, 0.308 a.u. at H$_{86}$–O$_{63}$ for LDP-HCO-Pt@C$_{60}$, 0.577 a.u. at C$_9$–H$_{81}$ for LDP-NH$_2$-Pt@C$_{60}$, 0.827 a.u. at O$_{84}$–C$_9$ for LDP-NO$_2$-Pt@C$_{60}$ and 0.433 a.u. at H$_{63}$–O$_{83}$ for LDP-OH-Pt@C$_{60}$. As stated in the literature, $\rho(r) > 0$; $\nabla^2\rho(r) > 0$ indicates the presence of a potent noncovalent bond, $\rho(r) < 0$; $\nabla^2\rho(r) < 0$ indicates the presence of a covalent interaction, and when $\rho(r) > 0$; $\nabla^2\rho(r) < 0$ indicates an existing partial covalent interaction between and within the studied complexes.[43]

Table 3 The summarized results of the computed adsorption energy calculated *via* the DFT/PBE1PBE/GENECP level of theory

Complexes	E_{complex}	E_{surface}	E_{gas}	E_{ad} (Ha)	E_{ad} (eV)	E_{ad} (kcal mol^{-1})
LDP-COOH-Pt@C$_{60}$	−3293.664154	−2589.674077	−704.510086	0.5200	14.15	326.3
LDP-HCO-Pt@C$_{60}$	−3218.511165	−2514.540275	−704.510086	0.53922	14.67	338.4
LDP-NH$_2$-Pt@C$_{60}$	−3160.657245	−2456.690070	−704.510086	0.5429	14.77	340.7
LDP-NO$_2$-Pt@C$_{60}$	−3309.537076	−2605.565038	−704.510086	0.5381	14.64	337.6
LDP-OH-Pt@C$_{60}$	−3180.497622	−2476.520130	−704.510086	0.5326	14.49	334.2

Table 4 Results for selected QTAIM parameters of the studied complexes calculated at DFT/PBE1PBE/GENECP level of theory[a]

System	Bond	BCP	$\rho(r)$	$\nabla^2\rho(r)$	$G(r)$	$K(r)$	$V(r)$	$H(r)$
LDP-COOH-Pt@C$_{60}$	C$_{62}$–C$_6$	152	0.232	−0.468	0.578	0.175	−0.233	−0.175
	H$_{73}$–N$_{88}$	96	0.799	0.354	0.662	−0.223	−0.439	0.223
	C$_{80}$–C$_{84}$	126	0.240	−0.506	0.608	0.187	−0.248	−0.187
LDP-HCO-Pt@C$_{60}$	H$_{72}$–N$_{87}$	93	0.128	0.542	0.109	−0.265	−0.825	0.265
	O$_{84}$–H$_{64}$	148	0.167	0.762	0.159	−0.318	−0.127	0.318
	H$_{86}$–O$_{63}$	94	0.308	0.109	0.264	−0.786	−0.256	0.786
LDP-NH$_2$-Pt@C$_{60}$	C$_9$–O$_{84}$	221	0.406	0.166	0.306	−0.109	−0.197	0.109
	H$_{64}$–O$_{84}$	247	0.195	0.886	0.193	−0.283	−0.165	0.283
	C$_9$–H$_{81}$	195	0.577	0.231	0.415	−0.162	−0.253	0.162
LDP-NO$_2$-Pt@C$_{60}$	O$_{84}$–N$_{62}$	220	0.100	0.464	0.905	−0.255	−0.650	0.255
	H$_{86}$–O$_{64}$	248	0.252	0.925	0.219	−0.122	−0.207	0.122
	O$_{84}$–O$_9$	180	0.827	0.410	0.763	−0.262	−0.501	0.262
LDP-OH-Pt@C$_{60}$	C$_9$–O$_{83}$	238	0.289	−0.744	0.986	0.285	−0.383	−0.285
	H$_{63}$–O$_{83}$	216	0.433	0.154	0.395	0.958	−0.405	−0.958
	C$_{78}$–N$_{86}$	241	0.263	−0.512	0.130	0.258	−0.387	−0.258

[a] The units of the parameters in Table 4 are as follows: $P(r)$, e/Ang^3; $\nabla^2\rho(r)$, e/Ang^3; $G(r)$ and $V(r)$ have units of eV; $H(r)$ has a unit of eV Ang^3/e.

Here, as shown in Table 4, all $\rho(r)$ values for the systems are greater than zero and positively charged, and the Laplacian of the electron density withholds a larger number of positive values greater than zero. This indicates a stronger presence of noncovalent interactions within the studied complexes, with LDP-NO$_2$-Pt@C$_{60}$ withholding the highest value and LDP-COOH-Pt@C$_{60}$ having a minimal interaction. The positive values of the Laplacian of electron density show that the complexes exhibit an electrostatic nature of interaction.[44] The degree of structural stability within the complexes can be estimated by the ellipticity of the electron density.[1,3] The greater the ellipticity of the electron density is, the lower the interaction stability. On average, the values are 0.45 a.u. for LDP-COOH-Pt@C$_{60}$, 0.008 a.u. for LDP-HCO-Pt@C60, 0.567 a.u. for LDP-NH$_2$-Pt@C$_{60}$, 0.785 a.u. for LDP-NO$_2$-Pt@C$_{60}$ and 0.112 a.u. for LDP-OH-Pt@C$_{60}$. Furthermore, the eigenvalues of the Hessian matrix (λ_1/λ_3) are less than one, which implies the presence of stronger intermolecular forces on the interacting surfaces. The electron density of all the complexes except LDP-NH$_2$-Pt@C$_{60}$ is greater than 0.5 a.u., which, according to previous literature, indicates that the systems exhibit delocalized electrons within their molecules.

3.4.2 Reduced density gradient (RDG) analysis. Aside from investigating the electron charge transfer within molecules, it is paramount to investigate the nature of the bond in the molecules of a system. The forces of attraction can be categorized as weak or strong and exist in a variety of forms, where the van der Waals force is a weak force and the steric force is a strong force of attraction.[45] Reduced density gradient analysis is referred to as a noncovalent study (NCI) because of its specificity in identifying weak interactions required in an adsorption study to understand the sensation and adsorption level of the levodopa molecule using various modified systems.[46] The application of this technique has spread across various fields and research interests, such as environmental and toxicology studies, power industries, and drug delivery.[46,47] By employing a computational approach, NCI visualization was carried out, as shown in Fig. 4.

The VMD application was utilized, and its isosurfaces appeared in different colour ranges, each having valuable information that aided the clarity of this study.

These loop-colored isosurfaces enhance the comprehension and graphical representation of the interactions occurring within and between systems, as reported in the QTAIM study. By analyzing the 3D RDG plot, valuable insights into the nature and strength of the forces governing adsorption can be gained. Herein, red-colored regions represent a steric force of attraction known as an intense kind of attraction. The green region indicates the degree of van der Waals dispersion forces occurring in the molecules, and the blue isosurface patterns indicate the hydrogen bonds. All these forces contribute to the determination of the degree of adsorption between the adsorbent and adsorbate. In Fig. 4, complexes LDP-OH-Pt@C$_{60}$ and LDP-NH$_2$-Pt@C$_{60}$ appear to have a green colour that is sparsely scattered around the region of the levodopa compound, and this observation represents the presence of van der Waals dispersion. Furthermore, the LDP-NO$_2$-Pt@C$_{60}$ complex is characterized by van der Waals interactions with a slight steric force owing to the occurrence of greener isosurface and a slight appearance of red loops. Analysis of the red zones in the NCI plot is crucial for pinpointing the locations of high-strength attractive interactions responsible for anchoring the adsorbate molecule onto the surface. For the LDP-HCO-Pt@C$_{60}$ complex, the levodopa compound is marginally surrounded by red and blue colours, which may be caused by the electronegativity of the oxygen atom in the HCO functional group, whereas the platinum metal is primarily surrounded by a green colour. The –COOH-functionalized surface exhibited a sparse distribution of red and blue colours within and between upon interaction with our studied pharmaceutical pollutant. According to the observations in this study, the LDP-OH-Pt@C$_{60}$, LDP-NO$_2$-Pt@C$_{60}$, LDP-NH$_2$-Pt@C$_{60}$, and LDP-COOH-Pt@C$_{60}$ complexes are the most suitable systems for the adsorption of levodopa. In general, the presence of red regions near the interface between the levodopa and the tailored fullerene surfaces indicates strong attractive
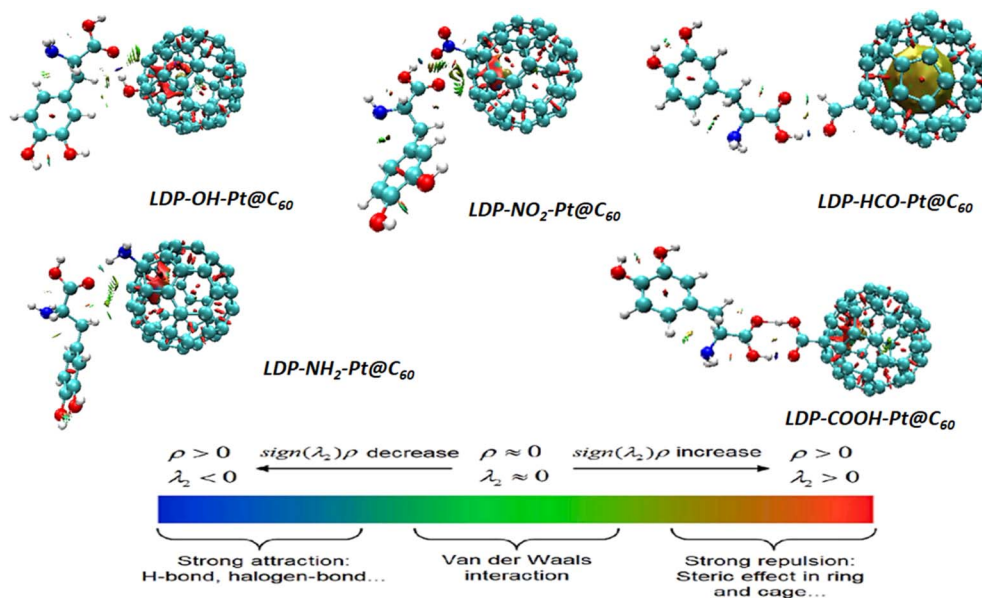
Fig. 4 3D-NCI plots for the studied complexes.

interactions that contribute significantly to adsorption strength. The presence of green regions, suggests additional dispersion forces contributing to the overall attraction brought by the adsorption configurations. Finally, specific hydrogen bonds further stabilizing the adsorbed levodopa can be pinpointed *via* the blue region.

3.5   Sensor properties

Categorizing sensor mechanisms based on their ability to provide insights into which materials are suitable for use as detectors and sensors in various systems is a step toward material commercialization. Oftentimes, it can be bothersome to show that some materials show a common tendency as sensors; however, their applicability has become a concern in engineering.[43] In the present section, an in-depth examination of the applicability of the labelled systems is carried out. The mechanisms discussed include electrical conductivity, charge transfer mechanism, work function, FET, and back donation.

3.5.1   Electrical conductivity. Electrical conductivity is the transfer of current from one end to the other over a surface in an electric field.[48] The formula employed for the electrical conductivity σ, holds at temperature T, energy gap E_g, constant K, and finally Boltzmann constant B, as presented in eqn (2):[49,50]

$$\sigma = AT^{2/3}e^{(E_g/2KT)} \qquad (2)$$

The conductivity can be related to the energy gap, so a small energy gap results in a high conductivity.[37] Table 5 shows how the energy gap changes as well as the percentage change in the energy gap. Due to the large percentage change in the energy gap obtained, it can be confirmed that the greatest change observed is due to the large changes as a result of the adsorption process. This in turn indicates the enhanced conductivity of the studied systems.

3.5.2   Charge transfer analysis and work function. Q_t is a result of inquiring into the distribution of electron densities. Herein, the natural charges of the adsorbent before and after adsorption were used to investigate the charge transfer mechanism. Eqn (3) (ref. 51) was used in the computation of the charge transfer (Q_t), and the results are summarized in Table 5. The schematic presentation of the formation of charge transfer between adsorbate and adsorbent is visualized in Fig. 5.

$$Q_t = Q_{adsorption} - Q_{isolated} \qquad (3)$$

Understanding this mechanism can be traced from the adsorbent to the adsorbate, and the other way around might be done using the plus and minus signs accompanying the magnitude of the charge transfer. Generally, electron transfer from the adsorbate to the adsorbent can be read as a negative Q_t, whereas a positive Q_t translates to the transfer of electrons from the adsorbent to the adsorbate.[52] In this work, electrons were transferred from the levodopa molecule to the adsorbents, except for LDP-NH$_2$-Pt@C$_{60}$, where electrons were transferred the other way around. Furthermore, it can be confirmed from Table 5 that the ϕ values computed are within a relatively small range of 7.421–7.591 eV, indicating little to no significant difference among the complexes. These results further show that the sensing attributes associated with the work function are nearly uniform among the labelled systems.

3.5.3   Fraction of electron transfer (FET) and back donation. The region of electron transfer from the functionalized surface to the levodopa gas can be understood using the fraction of electron transfer (FET) mechanism,[23,52] which can be written as ΔN. Gómez and coworkers established the possible contact that can exist between the adsorbent and the levodopa molecule during the adsorption process, thereby being

Table 5 Sensor properties calculated *via* the DFT/PBE1PBE/GENECP level of theory[a]

Systems	E_{ads}	ϕ	ΔE_g	% ΔE_g	Q_t	$\Delta E_{\text{back-donation}}$	ΔN
LDP-COOH-Pt@C$_{60}$	326.3	7.421	−0.8562	−85.62	−1.225	−0.03675	−0.47856
LDP-HCO-Pt@C$_{60}$	338.4	7.540	−0.8257	−82.57	−1.033	−0.03825	−0.37628
LDP-NH$_2$-Pt@C$_{60}$	340.7	7.423	−0.6683	−66.83	1.097	−0.08425	−0.35003
LDP-NO$_2$-Pt@C$_{60}$	337.6	7.591	−0.7919	−79.19	−0.908	−0.05175	−0.45978
LDP-OH-Pt@C$_{60}$	334.2	7.471	−0.7954	−79.54	1.208	−0.05125	−0.42598

[a] The units of E_{ad}, ΔE_g, ϕ, and $\Delta E_{\text{back-donation}}$ are in electron volt (eV). The Q_t has a unit of electron (e), and finally the % ΔE_g has its unit in percentage. ΔN is dimensionless.
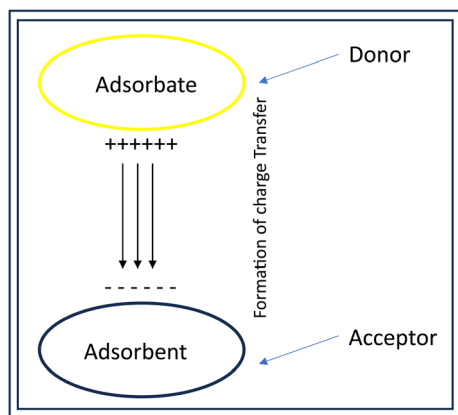
Fig. 5 Schematic presentation of the formation of charge transfer between adsorbate and adsorbent.

controlled by the use of the electrical back-donation mechanism.[53] Notably, the backward movement of electrons from levodopa to the labelled functionalized surface is known as back donation, and it is denoted as ΔE. The results computed at the DFT/PBE1PBE/GENECP level of theory are summarized in Table 5. Based on Pearson's theory, eqn (4) and (5) show how quantum descriptors can be related to ΔE and ΔN, respectively.[54,55]

$$\Delta N = \frac{\chi_{\text{isolated}} - \chi_{\text{system}}}{2\left(\eta_{\text{isolated}} - \eta_{\text{system}}\right)} \tag{4}$$

$$\Delta E_{\text{back donation}} = -\frac{\eta}{4} \tag{5}$$

According to eqn (4), a high ΔN may be achieved when the chemical hardness is low, which can further increase electron transfer during the adsorption process. Owing to a decrease in the tendency for charge transfer, the barrier to electron transfer can be improved. As expected for a material suitable for use as a sensor or detector device, back-donation is negative (that is, $\Delta E < 0$), and the chemical hardness is positive ($\eta > 0$).[44] Table 5 shows that the ΔE values are less than zero, indicating that the studied materials are good sensor materials. It is computationally necessary to say that a decrease in the η value will in turn reflect a corresponding decrease in stability. Additionally, high electron transfer from the surface to the adsorbate implies strong adsorption of the levodopa molecule, which can in turn

increase stability, provided that there is an increase in back donation.[42,44] LDP-COOH-Pt@C$_{60}$, LDP-NO$_2$-Pt@C$_{60}$, and LDP-OH-Pt@C$_{60}$ exhibited relatively high FET values of −0.47856, −0.45978, and −0.42598, respectively. This result confirmed the stability and relatively better adsorption in the aforementioned systems, confirming that the surfaces are suitable materials for detecting levodopa molecules, especially the COOH-Pt@C$_{60}$ surface.

3.6 Density of state (DOS) analysis

In computational studies, within the density functional theory framework, the density of states (DOS) analysis is vital in investigating and understanding the charge behaviors, flow, and transfer within atoms in a compound or material. The charge studies provide insights into the electron distribution which accounts for a percentage degree of interactions between the adsorbate and the adsorbent. Here, the energy sum in the materials is deciphered and the electrons transition from a ground state to an excited state is utilized in depicting the density of states level which directly affects and accounts for a material's behavior. Furthermore, the DOS analysis in a sense possesses a positive correlation with the patterns of electron shift in the HOMO–LUMO plots.

The DOS plots for all complexes are presented in Fig. 6. All surfaces possess a good percentage of carbon atoms and a platinum atom arising from the doping effect. The surfaces other than Pt-@C$_{60}$ possessed a range of atoms such as O, H, and N. In the plots. The atoms are represented in a colour tag with the total density of states (TDOS) above and the overlapping partial density of states (OPDOS) below, bearing the partial density of states (PDOS) between. The hydrogen atom possessed the least contribution and carbon the highest contribution with C falling within the lower range as compared to the TDOS. In the interaction plots, O possessed the peak in LDP-HCO-Pt@C$_{60}$, LDP-NO$_2$-Pt@C$_{60}$, LDP-NH$_2$-Pt@C$_{60}$, LDP-OH-Pt@C$_{60}$, interactions, and H possessed the highest in LDP-COOH-Pt@C$_{60}$. For all complexes, the Fermi energy level was present which is denoted as the average of the sum of the highest occupied molecular orbital (HOMO) and the lowest occupied molecular orbital (LUMO). Existing literature established that the distance of the Fermi energy level to the energy gaps affects the mobility of electrons.[56] A closer distance positions a faster transfer of electrons and *vice versa*. For all complexes plots, the Fermi-energy falls within the range of
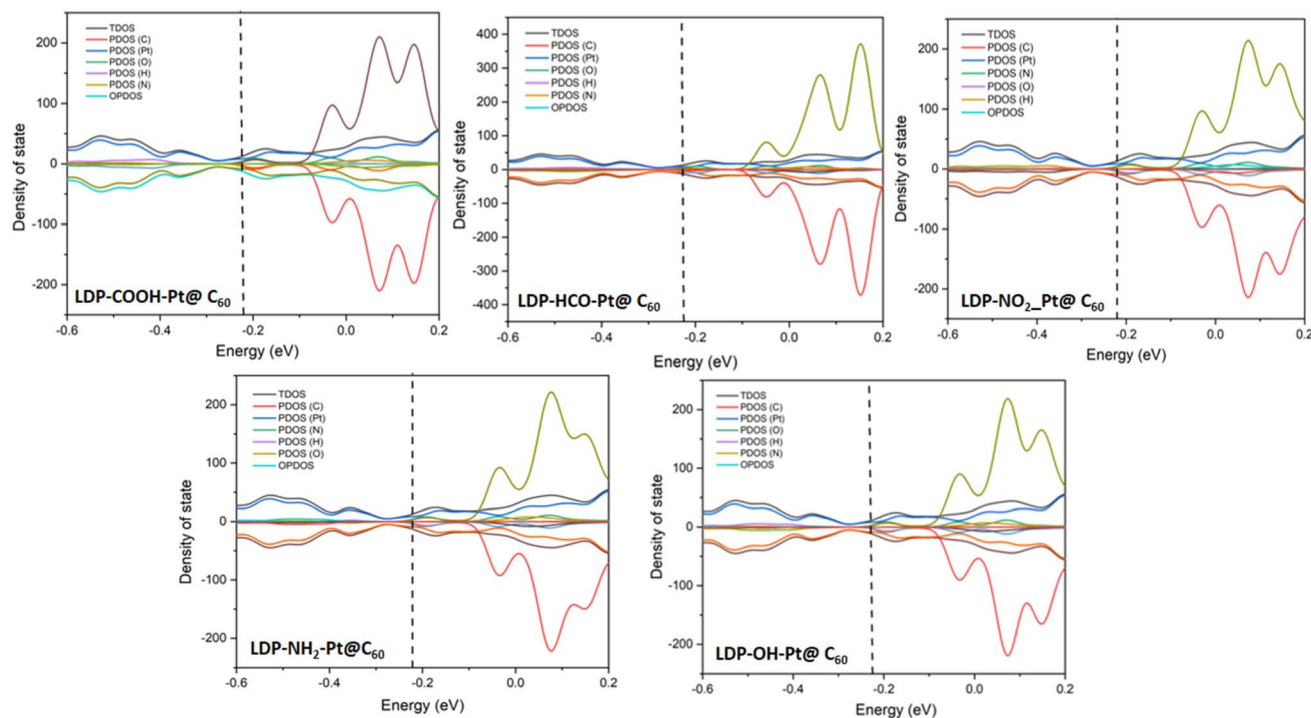
Fig. 6 Density of state plots showing the position of the TDOS, PDOS, and OPDOS of the studied surfaces upon adsorption.

−0.21 to −0.23 e.V with an energy gap range of 0.2 to 0.7 eV for interactions and 1.7–2.3 eV for surfaces. A closer distance in the Fermi-energy and energy gap is observed in the interacted surfaces which denotes a better electron activity likely occurred. Therefore, the results show an average distribution of charges has positively influenced the adsorption rate of the levodopa molecule on the adsorbents.

3.7 Molecular electrostatic potential (MESP)

As a valuable tool in molecular modelling of adsorption, MESP helps in understanding the distribution of electron density around a molecular system. This distribution influences how the molecule interacts with other molecules, including how strongly adsorption is onto a surface. Due to a negatively charged region of one molecule approaching a positively
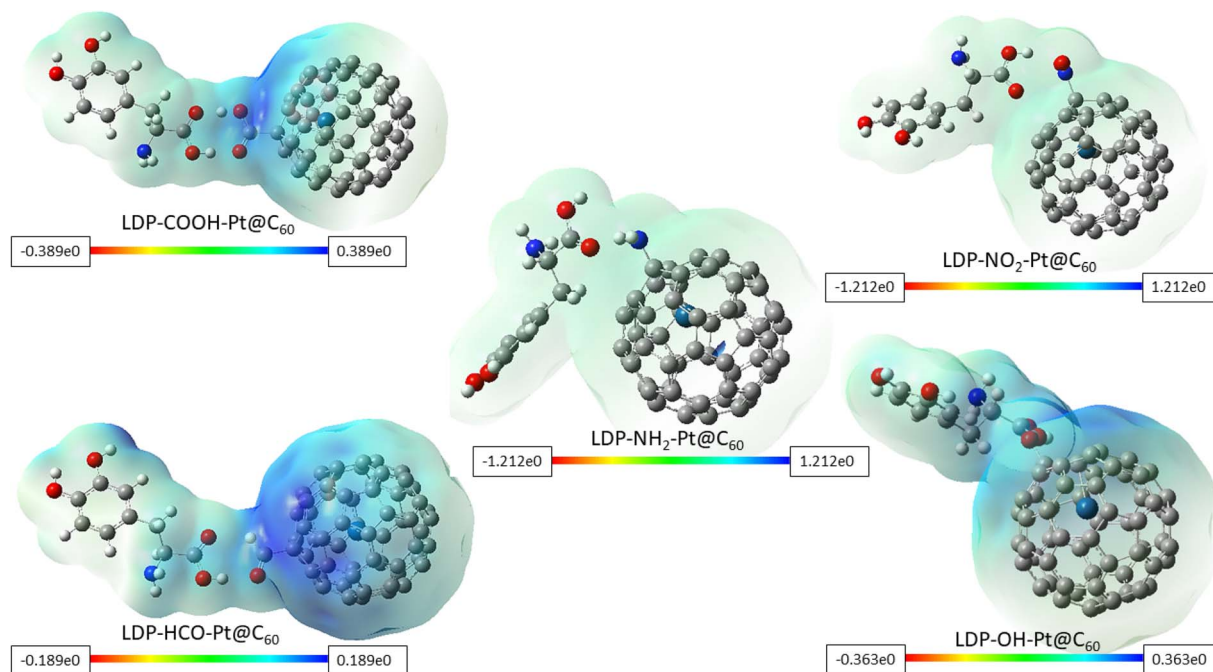

Fig. 7 Molecular electrostatic potential (MESP) maps of the studied surfaces upon adsorption.

charged region of another, an attractive force arises as a result of opposite charges.[57] This analysis enables one to identify these complementary regions and predict potential sites for favorable electrostatic interactions during adsorption. It also aids in predicting potential locations for hydrogen bonding. The hydrogen bonds are formed when a hydrogen atom bonded to a highly electronegative atom (like N, O, or F) interacts with another highly electronegative atom in a nearby molecule. Areas of high electron density are revealed around these electronegative atoms, thus showcasing potential sites for hydrogen bond formation during adsorption. Understanding the dipole–dipole interactions that occur between molecules with permanent electric dipoles contributes to the adsorption strength. Fig. 7 visualized the MESP maps for the investigated surfaces upon adsorption. The color scheme of the MESP maps is as follows: red color signifies electron-rich, partially negative charge; blue denotes electron-deficient, partially positive charge; yellow corresponds with slightly rich in electrons; and green implies neutral.[58] Electropositive and electronegative regions are encoded in blue and red colors respectively.[59] In Fig. 7, around complexes LDP-COOH-Pt@C_{60}, LDP-HCO-Pt@C_{60}, and LDP-OH-Pt@C_{60}, blue color can be seen near the area where –COOH, –HCO, and –OH groups functionalization took place, showing electrophilic characteristic. This is due to a result of the oxygen atom present in the functional groups, thereby creating a region of attractive electrostatic interaction. In addition, it can be inferred that electron density is in the aforementioned functional groups. The faint blue-green color observed in LDP-NH$_2$-Pt@C_{60}, and LDP-NO$_2$-Pt@C_{60}, around a region between the green and blue colors as shown in the maps (see Fig. 7), indicates a slightly deficient in electrons, approaching neutral. This suggests a combination of weak attractive and repulsive forces between the levodopa and the NH$_2$-Pt@C_{60} and NO$_2$-Pt@C_{60} adsorbents. This also reveals the presence of weak dispersion forces between the two interacting parties, arising from temporary fluctuations in electron density. Owing to the obtained results, it can be deduced in general, that adsorption of levodopa to the tailored surfaces is carried out from the region of the functional groups and adsorption strength is influenced by the varying electron-withdrawing abilities of the groups.

4 Conclusions

Investigation of the endohedral doping of a Pt atom on fullerene (C$_{60}$) followed by functionalization with specific groups (COOH, HCO, NH$_2$, NO$_2$, and OH) as adsorbents for levodopa was carried out using DFT/PBE1PBE/GENECP level of theory. Various theoretical analyses were thoroughly explored to gain insight into the electronic properties, nature of inter- and intra-molecular interactions, strength and phenomenal of adsorption, and the mechanisms of sensing. The following deductions have been drawn:

(I) The dimension elongated upon adsorption to 7.35 Å, 7.31 Å, 7.39 Å, 7.31 Å, and 7.39 Å for LDP-COOH-Pt@C_{60}, LDP-HCO-Pt@C_{60}, LDP-NH$_2$-Pt@C_{60}, LDP-NO$_2$-Pt@C_{60}, and LDP-OH-Pt@C_{60}, respectively. These changes in the dimensions are

attributed to the stretching vibration of the bonds in which the surfaces are made.

(II) All formed complexes exhibit of small energy gaps of 0.295 eV, 0.306 eV, 0.675 eV, 0.415 eV, and 0.409 eV, corresponding to the LDP-COOH-Pt@C_{60}, LDP-HCO-Pt@C_{60}, LDP-NH$_2$-Pt@C_{60}, LDP-NO$_2$-Pt@C_{60}, and LDP-OH-Pt@C_{60} complexes. This result indicates that electrons behave similarly in these materials, and exhibit a characteristic property of semi-conductors.

(III) The decreasing order of stabilization energies follows: LDP-OH-Pt@C_{60} > LDP-COOH-Pt@C_{60} > LDP-NH$_2$-Pt@C_{60} > COOH-Pt@C_{60} > LDP-NO$_2$-Pt@C_{60} > LDP-HCO-Pt@C_{60} > NO$_2$-Pt@C_{60} > OH-Pt@C_{60} > HCO-Pt@C_{60} > Pt@C_{60}. As compared to its studied counterparts, the LDP-OH-Pt@C_{60} will be easily stabilized during adsorption.

(IV) Since the energies are relatively close, the detection strength for levodopa follows the pattern LDP-COOH-Pt@C_{60} < LDP-OH-Pt@C_{60} < LDP-NO$_2$-Pt@C_{60} < LDP-NO$_2$-Pt@C_{60} < LDP-NH$_2$-Pt@C_{60}, which is a decreasing order of the detection strength.

(V) During AIM evaluation, in most cases, $\rho(r) > 0$ and $\nabla^2 \rho(r) > 0$ are obtained, indicating a stronger presence of noncovalent interactions which is in turn suitable for adsorption.

(VI) Deduction from MESP maps shows that adsorption of levodopa to the tailored surfaces is carried out from the region of the functional groups and adsorption strength is influenced by the varying electron-withdrawing abilities of the groups. This result was further substantiated using the 3D RDG maps in the NCI analysis.

(VII) Transfer of electrons occurred from the levodopa molecule to the adsorbents, except for LDP-NH$_2$-Pt@C_{60}, where electrons were transferred the other way around. LDP-COOH-Pt@C_{60}, LDP-NO$_2$-Pt@C_{60}, and LDP-OH-Pt@C_{60} exhibited relatively high FET values of −0.47856, −0.45978, and −0.42598, respectively, showcasing the stability and propensity of the labelled surfaces towards levodopa adsorption.

Data availability

All data are contained within the manuscript and manuscript ESI.† The available software used for the computational studies includes: Gaussian16 and GuassView6.0.16. Other software codes include: Chemcraft, Multiwfn analyser, and the Visual molecular dynamic (VMD) program, available at **http://sobereva.com/multiwfn/** and **https://www.ks.uiuc.edu/Research/vmd/**, respectively.

Conflicts of interest

No conflicts of interest.

References

1 A. Martínez, Dopamine delivery systems based on C60 and C24 with B and N as substituents, *Can. J. Chem.*, 2023, **101**(9), 595–602.

2 M. S. Raghu, L. Parashuram, K. Y. Kumar, B. P. Prasanna, S. Rao, P. Krishnaiah, K. N. Prashanth, C. P. Kumar and H. Alrobei, Facile green synthesis of boroncarbonitride using orange peel; its application in high-performance supercapacitors and detection of levodopa in real samples, *Mater. Today Commun.*, 2020, **24**, 101033.

3 J. Duhan and S. Obrai, Highly sensitive and selective fluorescence and smartphone-based sensor for detection of L-dopa using nitrogen sulphur graphene quantum dots, *Microchem. J.*, 2023, **193**, 109262.

4 P. A. LeWitt and S. Fahn, Levodopa therapy for Parkinson disease: a look backward and forward, *Neurology*, 2016, **86**(14_supplement_1), S3–S12.

5 A. Zhavoronkov, P. Mamoshina, Q. Vanhaelen, M. Scheibye-Knudsen, A. Moskalev and A. Aliper, Artificial intelligence for aging and longevity research: Recent advances and perspectives, *Ageing Res. Rev.*, 2019, **49**, 49–66.

6 D. G. Aaron, I. G. Cohen and E. Y. Adashi, The FDA struggle to withdraw Makena: problems with the accelerated approval process, *JAMA*, 2022, **328**(24), 2394–2395.

7 E. F. van Vliet, M. J. Knol, R. M. Schiffelers, M. Caiazzo and M. H. Fens, Levodopa-loaded nanoparticles for the treatment of Parkinson's disease, *J. Controlled Release*, 2023, **360**, 212–224.

8 F. Haddad, M. Sawalha, Y. Khawaja, A. Najjar and R. Karaman, Dopamine and levodopa prodrugs for the treatment of Parkinson's disease, *Molecules*, 2017, **23**(1), 40.

9 H. Bogetofte, A. Alamyar, M. Blaabjerg and M. Meyer, Levodopa therapy for Parkinson's disease: history, current status and perspectives, *CNS Neurol. Disord.: Drug Targets*, 2020, **19**(8), 572–583.

10 A. M. Richmond, K. E. Lyons and R. Pahwa, Safety review of current pharmacotherapies for levodopa-treated patients with Parkinson's disease, *Expert Opin. Drug Saf.*, 2023, **22**(7), 563–579.

11 M. P. Cruz, Pimavanserin (Nuplazid): a treatment for hallucinations and delusions associated with Parkinson's disease, *Pharm. Ther.*, 2017, **42**(6), 368.

12 R. García-Ramos, D. Santos-García, A. Alonso-Cánovas, M. Álvarez-Sauco, B. Ares, A. Ávila, N. Caballol, F. Carrillo, F. E. Sevilla, E. Freire and J. G. Esteban, Management of Parkinson's disease and other movement disorders in women of childbearing age: Part 1, *Neurologija*, 2021, **36**(2), 149–157.

13 M. Laipan, L. Xiang, J. Yu, B. R. Martin, R. Zhu, J. Zhu, H. He, A. Clearfield and L. Sun, Layered intercalation compounds: Mechanisms, new methodologies, and advanced applications, *Prog. Mater. Sci.*, 2020, **109**, 100631.

14 V. Ramezanzade, F. Mehvari, M. Dinari and S. ul Islam, Advances in Synthetic Methods, Surface Chemistry, and Characterizations of Fullerenes. InGreen Carbon Materials for Environmental Analysis: Emerging Research and Future Opportunities, *Am. Chem. Soc.*, 2023, 41–74.

15 A. V. Baskar, M. R. Benzigar, S. N. Talapaneni, G. Singh, A. S. Karakoti, J. Yi, A. A. Al-Muhtaseb, K. Ariga, P. M. Ajayan and A. Vinu, Self-assembled fullerene nanostructures: synthesis and applications, *Adv. Funct. Mater.*, 2022, **32**(6), 2106924.

16 V. Ramezanzade, F. Mehvari, M. Dinari and S. ul Islam, Advances in Synthetic Methods, Surface Chemistry, and Characterizations of Fullerenes. InGreen Carbon Materials for Environmental Analysis: Emerging Research and Future Opportunities, *Am. Chem. Soc.*, 2023, 41–74.

17 B. Petrovic, M. Gorbounov and S. M. Soltani, Influence of surface modification on selective CO2 adsorption: A technical review on mechanisms and methods, *Microporous Mesoporous Mater.*, 2021, **312**, 110751.

18 M. Li, R. Zhao, J. Dang and X. Zhao, Theoretical study on the stabilities, electronic structures, and reaction and formation mechanisms of fullerenes and endohedral metallofullerenes, *Coord. Chem. Rev.*, 2022, **471**, 214762.

19 H. S. Nafis, *Fundamentals of Organic Chemistry*, S. Chand Publishing, 2010.

20 A. M. Alsubaiyel, S. Alshehri, R. M. Alzhrani, A. D. Alatawi, M. A. Algarni, M. H. Abduljabbar, S. M. Alshahrani and N. B. Mohammed, Adsorption and electronic properties of pristine and Al-doped C60 fullerenes using N2O molecule: a theoretical study, *J. Mol. Liq.*, 2023, **369**, 120855.

21 H. Hadi, C. H. Lai, D. C. Agurokpon, H. C. de Oliveira and H. Louis, The effect of chemically functionalized C60-nanocages as sorbents and sensors for methamphetamine drug: A DFT and QTAIM study, *Diamond Relat. Mater.*, 2024, **141**, 110722.

22 F. Nattagh, S. Hosseini and M. D. Esrafili, Effects of B and N doping/codoping on the adsorption behavior of C60 fullerene towards aspirin: A DFT investigation, *J. Mol. Liq.*, 2021, **342**, 117459.

23 X. Liang, X. Tang, Y. Zhao, L. Zhang, Y. He and H. Li, High energy region formation with increased electron density located on the MoS2 layer within MoS2/Gr heterostructure induced by C60 decoration, *Surface. Interfac.*, 2023, **41**, 103237.

24 L. J. Ma, W. Hao, J. Jia and H. S. Wu, Sc/Ti-decorated and B-substituted defective C60 as efficient materials for hydrogen storage, *Int. J. Hydrogen Energy*, 2021, **46**(27), 14508–14519.

25 R. Sitko, M. Musielak, M. Serda, E. Talik, A. Gagor, B. Zawisza and M. Malecka, Graphene oxide decorated with fullerenol nanoparticles for highly efficient removal of Pb (II) ions and ultrasensitive detection by total-reflection X-ray fluorescence spectrometry, *Sep. Purif. Technol.*, 2021, **277**, 119450.

26 C. Parlak, Ö. Alver and Ö. Bağlayan, Quantum mechanical simulation of Molnupiravir drug interaction with Si-doped C60 fullerene, *J. Theor. Comput. Chem.*, 2021, **1202**, 113336.

27 M. J. Frisch, G. W. Trucks, H. B. Schlegel, G. E. Scuseria, M. A. Robb, J. R. Cheeseman, G. Scalmani, V. Barone, G. A. Petersson, H. Nakatsuji and X. Li, *Gaussian 16*, Rev. C. 01, Wallingford, CT. Wallingford, CT, 2016.

28 Q. Fatima, H. Zhang, A. A. Haidry, R. Hussain, R. A. Alshgari and S. Mohammad, Elucidating the optoelectronic properties Ag, Au and Pd doped graphene oxide using a DFT approach, *Diamond Relat. Mater.*, 2024, **146**, 111151.

29 E. D. Glendening, A. E. Reed, J. E. Carpenter and F. Weinhold, *NBO, Version 3.1*, Gaussian. Inc., Pittsburgh, PA, 2003.

30 J. Peng, Y. Zhao, X. Wang, X. Zeng, J. Wang and S. Hou, Metal-Organic Frameworks: Advances in First-Principles Computational Studies on Catalysis, Adsorption, and Energy Storage, *Mater. Today Commun.*, 2024, **6**, 109780.

31 R. Deji, A. Verma, N. Kaur, B. C. Choudhary and R. K. Sharma, Adsorption chemistry of co-doped graphene nanoribbon and its derivatives towards carbon based gases for gas sensing applications: quantum DFT investigation, *Mater. Sci. Semicond. Process.*, 2022, **146**, 106670.

32 T. Lu and F. Chen, Multiwfn: A multifunctional wavefunction analyzer, *J. Comput. Chem.*, 2012, **33**(5), 580–592.

33 W. Humphrey, A. Dalke and K. Schulten, VMD: visual molecular dynamics, *J. Mol. Graph.*, 1996, **14**(1), 33–38.

34 P. Chansoria, R. Rizzo, D. Rütsche, H. Liu, P. Delrot and M. Zenobi-Wong, Light from Afield: Fast, High-Resolution, and Layer-Free Deep Vat 3D Printing: Focus Review, *Chem. Rev.*, 2024, **124**(14), 8787–8822.

35 C. Wang, B. Wu and C. Wang, Rational Construction and Efficient Regulation of Stable and Long-Lived Charge-Separation State in Fullerene Materials, *Acc. Mater. Res.*, 2024, **5**(4), 426–437.

36 M. Doust Mohammadi and H. Y. Abdullah, The adsorption of chlorofluoromethane on pristine, and Al-and Ga-doped boron nitride nanosheets: a DFT, NBO, and QTAIM study, *J. Mol. Model.*, 2020, **26**, 1–5.

37 T. M. Alamgeer, M. R. Sarker, S. Ali, H. S. Ibraheem, S. Ali, M. Imran Khan, D. N. Khan, R. Ali and S. Mohd Said, Polyaniline/ZnO Hybrid Nanocomposite: Morphology, Spectroscopy and Optimization of ZnO Concentration for Photovoltaic Applications, *Polymers*, 2023, **15**(2), 363.

38 V. S. Tyurin, A. O. Shkirdova, O. I. Koifman and I. A. Zamilatskov, Meso-Formyl, Vinyl, and Ethynyl Porphyrins—Multipotent Synthons for Obtaining a Diverse Array of Functional Derivatives, *Molecules*, 2023, **28**(15), 5782.

39 J. Hong, J. Kwon, D. Im, J. Ko, C. Y. Nam, H. G. Yang, S. H. Shin, S. M. Hong, S. S. Hwang, H. G. Yoon and A. S. Lee, Best practices for correlating electrical conductivity with broadband EMI shielding in binary filler-based conducting polymer composites, *Chem. Eng. J.*, 2023, **455**, 140528.

40 S. J. Basha and S. V. Chamundeeswari, Quantum computational, spectroscopic and molecular docking studies of 5, 5-dimethylhydantoin and its bromine and chlorine derivatives, *Chem. Data Collect.*, 2020, **29**, 100461.

41 K. Cui, *Computational Modeling of the Acid Gas-induced Evolution in Metal-Organic Frameworks*, The University of Wisconsin-Madison, 2022.

42 A. Samanth, R. Vinayagam, G. Murugesan, T. Varadavenkatesan, R. Selvaraj and A. Pugazhendhi, Enhanced adsorption of 2, 4-dichlorophenoxyacetic acid using low-temperature carbonized Peltophorum pterocarpum pods and its statistical physics modeling, *Chemosphere*, 2023, **336**, 139143.

43 P. K. Anjalikrishna, S. R. Gadre and C. H. Suresh, Topology of electrostatic potential and electron density reveals a covalent to non-covalent carbon–carbon bond continuum, *Phys. Chem. Chem. Phys.*, 2023, **25**(37), 25191–25204.

44 H. Sajid, S. A. Siddique, E. Ahmed, M. Arshad, M. A. Gilani, A. Rauf, M. Imran and T. Mahmood, DFT outcome for comparative analysis of Be12O12, Mg12O12 and Ca12O12 nanocages toward sensing of N2O, NO2, NO, H2S, SO2 and SO3 gases, *J. Theor. Comput. Chem.*, 2022, **1211**, 113694.

45 U. Sohail, F. Ullah, T. Mahmood, S. Muhammad and K. Ayub, Adsorption of industrial gases (CH4, CO2, and CO) on olympicene: a DFT and CCSD (T) investigation, *ACS Omega*, 2022, **7**(22), 18852–18860.

46 M. D. Mohammadi, H. Y. Abdullah, K. W. Qadir and A. Suvitha, Theoretical investigation of intermolecular interactions between CNT, SiCNT and SiCGeNT nanomaterials with vinyl chloride molecule: a DFT, NBO, NCI, and QTAIM study, *Diamond Relat. Mater.*, 2023, **131**, 109602.

47 E. Nemati-Kande, M. Abbasi and M. D. Mohammadi, Feasibility of pristine and decorated AlN and SiC nanotubes in sensing of noble gases: a DFT study, *ChemistrySelect*, 2019, **4**(8), 2453–2462.

48 S. Haghgoo and A. R. Nekoei, Metal oxide adsorption on fullerene C 60 and its potential for adsorption of pollutant gases; density functional theory studies, *RSC Adv.*, 2021, **11**(28), 17377–17390.

49 A. Yadav, A. Taha, Y. A. Abdulsayed and S. M. Saeed, A Density Functional Theory (DFT) Study on Adsorption of a biological active ethionamide over the Surface of a Fe-decorated porphyrin system, *Chem. Rev. Lett.*, 2023, **6**(2), 128–138.

50 J. S. Al-Otaibi, Y. S. Mary, Y. S. Mary and A. A. Al-Saadi, Revealing the adsorption nature of disulfiram on metal clusters (Au, Pt, Ag, Pd, Cu, and Ni): DFT analysis, SERS enhancement and sensor properties, *J. Theor. Comput. Chem.*, 2024, **1235**, 114543.

51 M. Khnifira, S. El Hamidi, A. Machrouhi, A. Mahsoune, W. Boumya, H. Tounsadi, F. Z. Mahjoubi, M. Sadiq, N. Barka and M. Abdennouri, Theoretical and experimental study of the adsorption characteristics of Methylene Blue on titanium dioxide surface using DFT and Monte Carlo dynamic simulation, *Desalin. Water Treat.*, 2020, **190**, 393–411.

52 W. Hu, W. C. Cheng and S. Wen, Investigating the effect of degree of compaction, initial water content, and electric field intensity on electrokinetic remediation of an artificially Cu-and Pb-contaminated loess, *Acta Geotech.*, 2023, **18**(2), 937–949.

53 Y. Yang, F. Y. Gao, X. L. Zhang, S. Qin, L. R. Zheng, Y. H. Wang, J. Liao, Q. Yang and M. R. Gao, Suppressing Electron Back-Donation for a Highly CO-tolerant Fuel Cell Anode Catalyst via Cobalt Modulation, *Angew. Chem., Int. Ed.*, 2022, **61**(42), e202208040.

54 M. Abreu-Quijano, M. Palomar-Pardavé, A. Cuán, M. Romero-Romo, G. Negrón-Silva, R. Álvarez-Bustamante, A. Ramírez-López and H. Herrera-Hernández, Quantum chemical study of 2-mercaptoimidazole, 2-Mercaptobenzimidazole, 2-Mercapto-5-Methylbenzimidazole and 2-Mercapto-5-Nitrobenzimidazole as corrosion inhibitors for steel, *Int. J. Electrochem. Sci.*, 2011, **6**(9), 3729–3742.

55 H. Challouf, N. Souissi, M. B. Messaouda, R. Abidi and A. Madani, Origanum majorana extracts as mild steel corrosion green inhibitors in aqueous chloride medium, *J. Environ. Prot.*, 2016, **7**(04), 532.

56 S. Sun, B. Peng, Y. Song, B. Liu, H. Song and W. Lin, Boosting photoelectron transfer by Fermi and doping levels regulation in carbon nitride towards efficient solar-driven hydrogen production, *Chem. Eng. J.*, 2024, **495**, 153547.

57 M. Arfan, I. M. Telles and A. P. dos Santos, Strong attraction between like-charged metal nanoparticles mediated by multivalent counterions, *J. Mol. Liq.*, 2024, **401**, 124527.

58 M. A. Sakr, M. A. Saad, V. A. Saroka, H. Abdelsalam and Q. Zhang, Exploring the potential of chemically modified graphyne nanodots as an efficient adsorbent and sensitive detector of environmental contaminants: a first principles study, *J. Fluoresc.*, 2024, **34**(2), 945–960.

59 B. Kumar, J. Devi, A. Dubey, N. Tufail and D. Khurana, Thiosemicarbazone ligands based transition metal complexes: A multifaceted investigation of antituberculosis, anti-inflammatory, antibacterial, antifungal activities, and molecular docking, density functional theory, molecular electrostatic potential, absorption, distribution, metabolism, excretion, and toxicity studies, *Appl. Organomet. Chem.*, 2024, **38**(3), e7345.